CRYSTAL GROWTH & DESIGN

Article

Morphological control of InN nanorods by SAG-HVPE

Mohammed ZEGHOUANE, Geoffrey Avit, Yamina ANDRE, Thierry Taliercio, Pierre Ferret, Evelyne Gil, Dominique CASTELLUCI, Pierre DISSEIX, Joel LEYMARIE, Eric Tournié, and Agnes Trassoudaine

Cryst. Growth Des., **Just Accepted Manuscript** • DOI: 10.1021/acs.cgd.9b01346 • Publication Date (Web): 20 Feb 2020

Morphological control of InN nanorods by SAG-HVPE

Mohammed Zeghouane *[a], *Geoffrey* Avit [a], *Yamina* André [a,b], , *Thierry* Taliercio [c], *Pierre* Ferret [d], *Evelyne* Gil [a,b], *Dominique* Castelluci [a], *Pierre* Disseix [a], *Joel* Leymarie [a], *Eric* Tournié [c], and *Agnès* Trassoudaine *[a]

[a] Université Clermont Auvergne, CNRS, SIGMA Clermont, Institut Pascal, F-63000 Clermont-Ferrand, France
[b] ITMO University, Kronverkskiy prospekt 49, 197101 St. Petersburg, Russia
[c] IES, Univ. Montpellier, CNRS, F-34000, Montpellier, France
[d] CEA-DRT LETI/DTS, 17 rue des Martyrs 38054 Grenoble, France

Abstract

The control of the morphology of InN nanorods, which remains challenging due to complex mechanisms involved in the growth process, is essential for the next generation of nano- and optoelectronic devices. In this paper, we report on the Selective Area Growth (SAG) of InN nanorods on Ga-polar GaN/c-Al_2O_3 template using Hydride Vapor Phase Epitaxy (HVPE). A systematic study of the evolution of the shape of InN nanorods under various growth conditions: growth temperature, growth time and the input NH_3 partial pressure, is carried out. The optimal growth temperature to achieve a perfect selectivity and prevent InN decomposition is first determined. The axial and radial growth rates dependence on the growth temperature and vapor phase composition with group V elements is discussed. The influence of mass transport on the InN nanorods geometry is shown to be more pronounced at extended growth time. The swapping of the nanorods morphology from pencil to a perfect hexagonal shape is controlled by varying the growth time. Photoluminescence measurements on InN nanorods are interpreted by considering a concentration of free electrons. The results reported herein provide relevant information for understanding SAG of InN, and could pave the way to develop high performance InN nanorods based devices.

Keywords: Hydride Vapor Phase Epitaxy, Indium Nitride, Selective Area Growth, Nanorods

1. Introduction

The III-nitride materials are promising for applications such as light emitting diodes, laser diodes, high power transistors and photovoltaic [1]. In fact, the binary InN material has unique and excellent intrinsic properties with the narrowest band gap of all the III-nitride family, low effective mass and a large drift-velocity, making it an ideal candidate for infrared light emitters and high-speed electronic devices [2], [3], [4], [5], [6]. However, the growth of high-quality InN layers is hampered by the high lattice mismatch with usual substrates [2], [7], [8], [9], [10], [11]. In an effort to circumvent this limitation, the 1D geometry of nanowires is used [12]. The small footprint on the substrate surface allows to improve the crystal quality and reduce the dislocation density through the effective stress relaxation [13]. Furthermore, the nanowire specific surface is larger than that of planar layers which is beneficial to enhance terahertz (THz) wave emission [14] and increases light output of LED devices [15]. The most widely used methods to grow nitride nanowires are Au-catalysed and self-catalysed growths. These growth techniques yield poor uniformity and random growth directions, while deep level defects due to the incorporation of the metal catalyst are observed in the materials [16], [17]. These issues can be addressed by the catalyst-free selective area growth (SAG) technique. Precise control of the size and the position of wires can be achieved by using openings on a dielectric mask defined by lithography. This approach is based on the difference of the nucleation barrier between the mask and the substrate.

Until now few studies have been reported on the SAG of InN nanorods due to challenges faced in obtaining a good selectivity with a high crystal quality. It is difficult to obtain a perfect selectivity in the usual temperature range for growing InN. To the best of our knowledge, the SAG of InN by metal organic vapour phase epitaxy (MOVPE) has never been reported. In molecular beam epitaxy (MBE), the growth of InN nanorods with a good selectivity was achieved. However, it is very difficult to control the morphological shape with a well-defined aspect ratio because of the complexity of InN growth kinetics [18], [19], [20], [21]. The perfect selective area growth of vertically aligned InN nanorods with a high aspect ratio was newly demonstrated thanks to the Hydride Vapour Phase Epitaxy (HVPE) process [22]. The SAG was performed on SiN masked Ga-polar GaN/c-Al_2O_3 templates with circular openings of 200 nm. It resulted in perfectly hexagonal InN nanorods delimited with (1-100) m-planes, (11-20) a-planes and the top (0001) c-plane. However, it was reported that the optical and electrical properties of 1D nitride structures may heavily depend on their shape [23]. Indeed, the photoluminescence (PL) emission of InN nanorods or

nanowires critically relies on their crystal quality and morphology (length-diameter-facets) [24], [25]. That is why the control of the hierarchy of the growth rates of the different nanorod facets and thereby the control of the final shape is of utter interest.

Crystal shape engineering of nitride structures by SAG-HVPE can be carried out by varying the vapor phase composition and the growth temperature. These experimental parameters govern the kinetics involved in the growth process [26], [27], [28]. Understanding how each parameter impacts the crystal growth of InN is important to monitor the form of nanorods. To the best of our knowledge, no study has ever been carried out to understand and ultimately control the SAG of InN nanorods. Therefore, it is timely to conduct detailed and systematic studies of the SAG of InN nanorods which is the aim of this work.

The effect of the growth temperature on the selectivity and the growth rates is first investigated. Then, the impact of the partial pressure of the V element on the morphology of rods is studied, as well as the evolution of the growth rates over time. Finally, the optical quality of grown InN nanorods is assessed by photoluminescence spectroscopy.

2. Experiment

The SAG of InN nanorods was carried out in a 2-inch quartz reactor at atmospheric pressure placed in three-zone horizontal furnace. In the first zone, called the source zone, indium tri-chloride ($InCl_3$) gaseous species were formed in a quartz boat by sublimation of an $InCl_3$ powder conducted by a nitrogen flux (N_2) between 450 °C and 500 °C. Ammonia (NH3) was directly introduced into a central zone heated at a higher temperature for an efficient mixing of the gas species. The spot at higher temperature also suppresses the parasitical nucleation upstream the sample. The third zone is the growth zone. Ultra-high purity nitrogen (N_2) is used as carrier gas. *C*-plane sapphire templates, covered with a 4 µm-thick Ga-polar buffer layer and masked with SiNx, were used as substrates. The pattern was defined with nano-imprint lithography (NIL) and consisted of arrays of circular holes of 200 nm spaced 2 µm apart. Nanorods morphologies, including diameters and heights were studied by Carl Zeiss Supra Scanning Electron Microscope (SEM) using an acceleration voltage of 3 kV. The optical properties were analyzed by Photoluminescence spectroscopy (PL) using an excitation wavelength of 780 nm, focused on

nanorods ensemble with a spot of 200 μm. The luminescence signal was detected through a Fourier-transform infrared spectrometer using a liquid-N_2-cooled InSb detector.

3. Results and discussion

The growth morphology of InN nanorods is sensitive to several factors, mainly the growth temperature and the V/III ratio. The growth temperature affects the crystal growth of InN material, both the crystal quality and the growth rates, while insuring at the same time a good selectivity on the mask. Consequently, we first systematically studied the effect of this key parameter by fixing all other growth conditions. The input partial pressures of NH_3 (P^0_{NH3}) and $InCl_3$ (P^0_{InCl3}) were respectively kept at 1.00 x 10^{-1} atm and 1.38 x 10^{-3} atm yielding to V/III ratio of about 72. These partial pressures were initially inspired by the work in Ref [22]. The growth temperature was varied from 580 °C to 690 °C in order to define the temperature window of the SAG regime. The choice of this range of temperature was imposed by the decomposition temperature of InN. On the other hand, the partial pressure of NH_3 is considered as one of the most impacting parameters on InN growth due to the weak nature of the In-N bond but also to the addition of hydrogen coming from its decomposition. To understand the SAG of InN nanorods, a study as a function of P^0_{NH3} was also carried out. The growth temperature was kept at 640 °C and the growth time was 5 minutes.

Furthermore, several studies on SAG have shown that the grown nanostructures undergo morphological evolution from the initial to the stable shape driven by free-energy minimization [28]. To gain a further understanding of the SAG growth of InN nanorods, additional experiments were carried out by varying the growth time. The growth temperature was 640 °C, P^0_{NH3} and P^0_{InCl3} were respectively kept at 1.00 x 10^{-1} atm and 1.38 x 10^{-3} atm. For a better understanding of the impact of each growth parameter, the diameter of the mask holes and the spacing between apertures were fixed for the whole work.

- **Effect of the growth temperature**

Figures 1 (a) to (e) show tilted-view SEM images of samples grown for 30 minutes at different growth temperatures: T_1 = 580 °C, T_2 = 610 °C, T_3 = 640 °C, T_4 = 660 °C and T_5 = 690 °C. It is clear that the selectivity and the growth rates are dependent on the growth temperature showing a noticeable effect on the geometry of InN nanorods obtained by SAG. At a growth temperature of

580 °C, random nucleation of InN occurs on the mask as shown in Figure 1 (a). When the growth temperature is higher than 610 °C, the growth of vertically aligned InN nanorods with a perfect selectivity becomes favorable. Previous reports dealing with SAG of nitrides by MBE and MOVPE, have shown that selectivity is driven by the surface diffusion of adatoms and their probability to reach the mask holes is enhanced at high growth temperatures [29], [30]. The special feature of HVPE when it comes to selective epitaxy is the low adsorption of chloride growth species on the dielectric mask. The uniform diameter of the nanorods shows that growth is not supplied with ad-species on the mask. The growth of nanorods results mainly from direct condensation of species from the vapour phase. Growth is then governed by the kinetics of adsorption, desorption, dechlorination and surface diffusion on the growing crystal facets, as we discuss below. The nanorods diameter is larger than the mask hole because of the epitaxial lateral growth, which was already observed in SAG of nitride materials. [31], [32], [33]

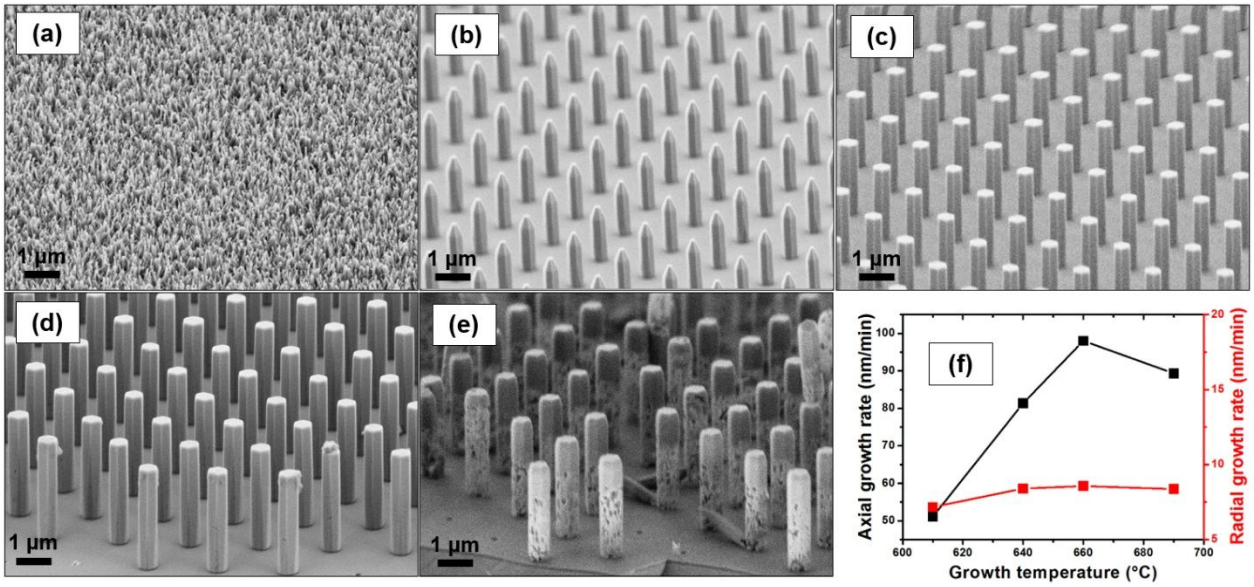

Figure 1: (a) – (e) SEM images of InN nanorods grown on Ga polar GaN/c-Al_2O_3 templates masked by SiN_x at growth temperatures of (a) 580 °C, (b) 610 °C, (c) 640 °C, (d) 660 °C and (e) 690 °C. (f) Axial (black) and radial (red) growth rates of InN nanorods as a function of the growth temperature. The selectivity is achieved from 610 °C. The higher growth temperature of 690 °C results in InN crystal deterioration.

The axial and radial growth rates of InN nanorods as a function of the growth temperature deduced from SEM images are presented in Figure 1 (f). The relative lengths of InN nanorods

grown at 610 °C, 640 °C, 660 °C and 690 °C are 1.53 µm, 2.44 µm, 2.95 µm and 2.68 µm, respectively. The axial growth rate of InN nanorods gradually increases from 51 $nm.mn^{-1}$ to 98 $nm.mn^{-1}$ when the growth temperature increases from 610 °C to 660 °C and then decreases to 87 $nm.mn^{-1}$ at 690 °C. Several studies on InN layer grown by MOVPE, MBE and HVPE shows similar "bell-shaped" curve of the growth rate as a function of the growth temperature [2]. At temperatures between 610 °C and 660 °C, growth is mainly limited by the adsorption and dechlorination kinetics, and to a lesser extent by the kinetics of surface diffusion of the ad-species on the crystal facets, which all depend on the temperature, dechlorination and surface diffusion being activated upon temperature. Consequently, the axial growth rate shows a strong positive variation with the temperature. At high growth temperature of 690 °C, desorption is favored over adsorption and growth becomes simply limited by the lack of material. At the same time, InN crystal decomposition is enhanced at this temperature due to the weak In-N bond (Figure 1 (e)). As a consequence, the axial growth rate decreases. On the over hand, the radial growth rate remains low and varies slightly with the growth temperature. The relative diameters of InN nanorods grown at 610 °C, 640 °C, 660 °C and 690 °C are 0.45 µm, 0.55 µm, 0.58 µm and 0.56 µm, respectively. The morphology of InN nanorods changes from pencil-like shape (Figure 1 (b)) to a perfect hexagonal pillar surrounded by the vertical (1-100) and (11-20) facets and (0001) top facet (Figure 1 (c)) by increasing the growth temperature from 610 °C up to 640 °C. The angle for the side edge referring to the (0001) plane in Figure 1(b) is 63 ± 2° which corresponds to the (1-101) r-plane facet of wurtzite InN. The existence of such morphologies is related to the anisotropic growth rates of the different facets [28]. The disappearance of the r-planes facets at higher growth temperature of 640 °C is probably due to an increase in their growth rate with respect to the c-plane facet, as will be seen below.

- **Effect of the input NH_3 partial pressure**

Bird's eye view SEM images of the samples grown for 5 minutes with 5.00 x 10^{-2} atm, 1.00 x 10^{-1} atm, 1.50 x 10^{-1} atm and 2.00 x 10^{-1} atm of P^0_{NH3} are shown in Figures 2 (a), (b), (c), (d) respectively. Clearly, selectivity is achieved for all samples whatever $P^0_{NH3,}$ unlike what was observed in previous MBE studies where selectivity has been shown to depend on the V/III ratio. For example, Kamimura et al [19] showed that the selectivity of InN nanorods grown by MBE was improved under In-rich conditions, allowing indium adatoms to easily diffuse on the mask

surface and reach the holes before reacting with nitrogen to yield spontaneous nucleation of InN on the mask. The absence of any InN nucleation on the mask surface at high NH_3 partial pressure confirms the low adsorption of III-chlorides species on the dielectric mask in the HVPE process.

Also, there is a clear transition in the axial growth rate as a function of P^0_{NH3} as plotted in Figure 2 (e) while the radial growth decreases very slightly. For a low P^0_{NH3} of 5.00 x 10^{-2} atm supplied in the vapor phase (Figure 2 (a)), the axial growth rate is equal to 320 nm.min^{-1}. An increase of P^0_{NH3} enhances the axial growth rate to reach the maximum 362 nm.min^{-1} at 1.00 x 10^{-1} atm (Figure 2 (b)). Then, it decreases for higher P^0_{NH3} as seen in Figure 2 (c) and (d).

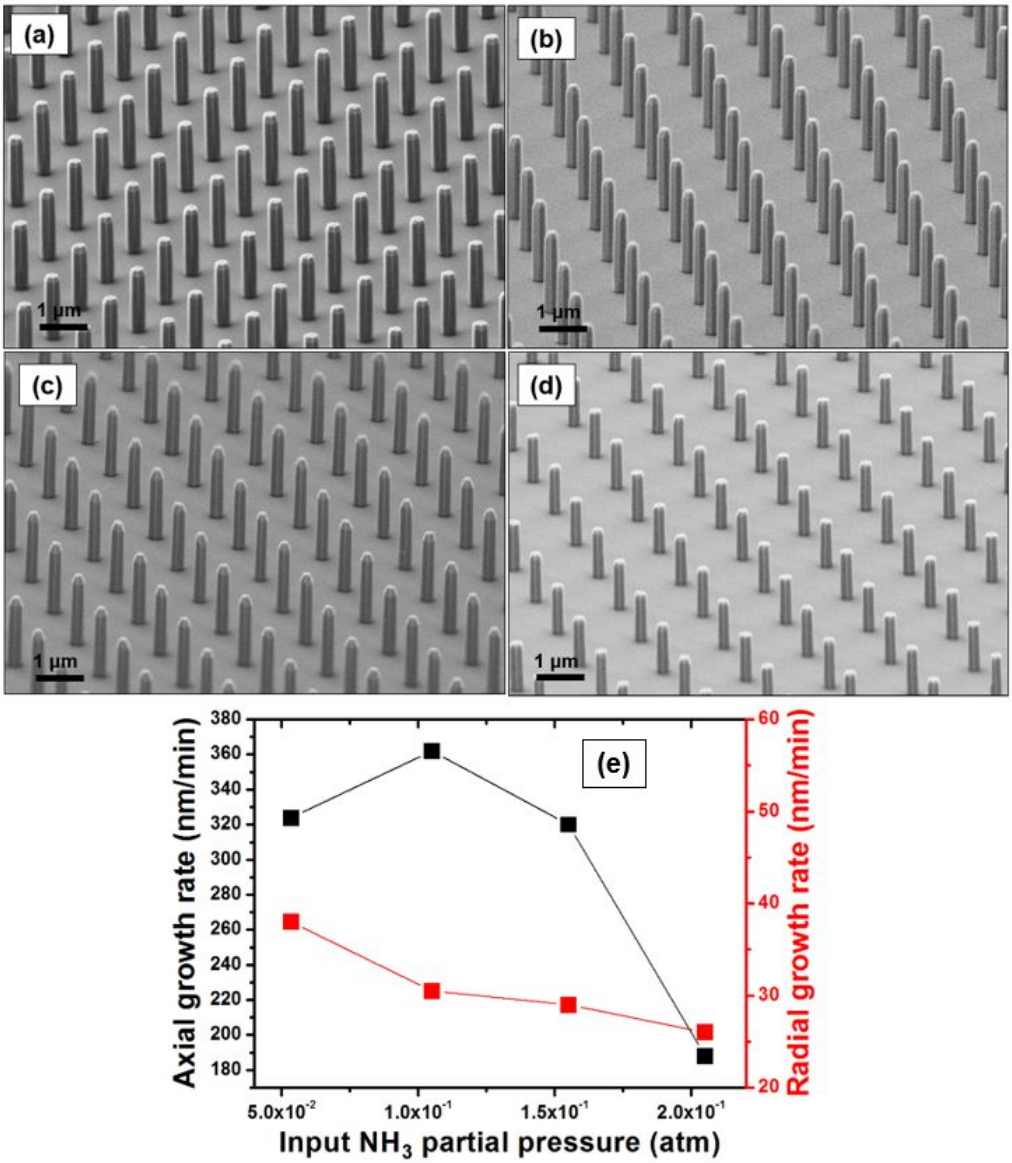

Figue 2: (a) – (d) SEM images of InN nanorods grown on Ga polar GaN/c-Al_2O_3 templates masked by SiN_x at different input NH_3 partial pressures (a) 5.00 x 10^{-2} atm, (b) 1.00 x 10^{-1} atm, (c) 1.50 x 10^{-1} atm and (d) 2.00 x 10^{-1} atm. (e) Axial (black) and radial (red) growth rates of InN nanorods as a function of the input NH_3 partial pressure. Nanorods growth rate and morphology depend on the introduced partial pressure of NH_3.

To further explain these observations, the supersaturation parameter is introduced. It represents the state of the growth reaction: $InCl_3 + NH_3 \leftrightarrow InN + 3\ HCl$ with respect to its equilibrium. The supersaturation is defined as the ratio of the real partial pressures P_i above the substrate with respect to the partial pressures of equilibrium:

$$\gamma_{InN} = \frac{P_{InCl3}\, P_{NH3} K}{P_{HCl}^3} - 1 \qquad (1)$$

where K is the equilibrium constant calculated from thermochemical data. Further details on thermodynamic calculation can be found in Ref [34].

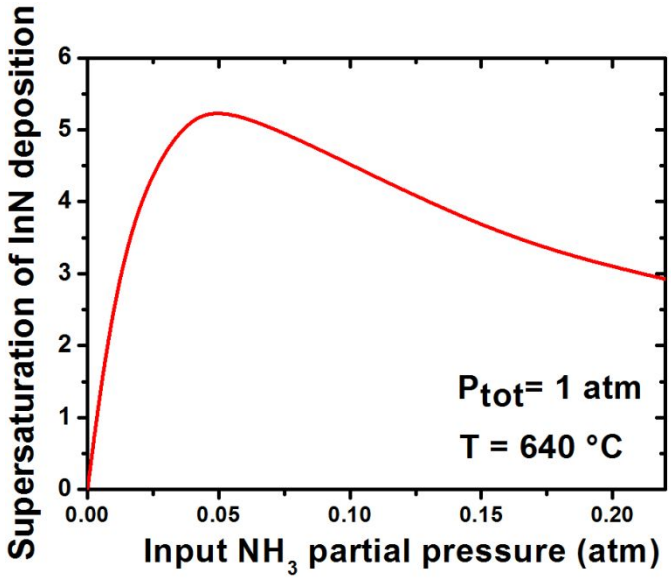

Figure 3: Plot of the supersaturation parameter for InN deposition as a function of the input NH_3 partial pressure. P_{tot} is the total pressure in the reactor. The supersaturation in the vapor phase to promote InN deposition decreases at higher P^0_{NH3}.

The supersaturation in the vapour phase above the substrate needed to promote InN crystal growth is plotted in Figure 3. The supersaturation increases with the supply of NH_3, until a peak

value where it begins to decrease. When P^0_{NH3} increases, hydrogen species produced by the dissociation of ammonia in the mixing zone increases and react quasi-totally with $InCl_3$ before deposition according to the following reaction:

$$InCl_{3(g)} + H_{2(g)} \leftrightarrow InCl_{(g)} + 2HCl_g \quad (2)$$

Yet, InCl molecules are not involved in the growth of InN due to their low reactivity towards NH_3, as previously demonstrated by Koukitu et al [35]. At the same time, this reaction is counterbalanced by the formation of HCl species in the vapour phase. As a consequence, the supersaturation of InN deposition decreases and the axial growth rate decreases at higher P^0_{NH3}. Similar findings were observed with respect to the effect of H_2 on the growth rate of InN films grown by HVPE [2], [35]. Other studies by MOVPE showed that the effect of NH_3 on the growth rate of InN layers is linked to the growth temperature since NH_3 decomposition kinetics depends mainly on this parameter [2]. In the HVPE process, the growth temperature, which is higher than 600 °C, is supposed to be high enough to overcome this limitation. Furthermore, previous studies demonstrated that the radial growth rate of GaN rods grown by HVPE decreases at a high partial pressure of HCl and/or H_2 [26], [27]. These findings are in accordance with the theoretical results dealing with the effect of H_2 on the growth rate of non-polar GaN (1-100) surfaces [36]. In that sense, we suppose that such decrease of the radial growth rate of InN nanorods can be related to the additional HCl in the vapour phase formed by reaction (2) and/or H_2 produced by NH_3 dissociation. This supports the fact that the lateral growth rate of nanorods grown in this study remains low whatever the V/III ratio and the growth temperature.

KOH etching in aqueous solution at 40 °C, which is known to etch only N-polar surfaces, reveals that the InN nanorods have In-polarity on the (0001) top facet, indicating that (1-101) r-planes surfaces are nitrogen-terminated. It has been pointed out by several works that hydrogen can easily passivate the N-terminated surfaces [37]. Under our growth conditions we believe that the r-planes can be passivated by H atoms originating from the NH_3 decomposition and forming N-H bonds, which leads to stable (1-101) r-planes facets. However, contrary to what was foreseen, the r-planes facets disappear at higher P^0_{NH3} of 2.00×10^{-1} atm as we can see in Figure 2 (d). According to Wulff theory of crystal growth, we assume that the disappearance of the (1-101) r-planes facets at this high P^0_{NH3} is related to the reduced growth rate of the (0001) c-plane facet.

This disappearance of the r-planes facets in favor of the c-plane is in agreement with the effect of the growth time as presented below.

- **Evolution of the morphology of InN nanorods with the growth time**

The typical morphologies of InN nanorods grown at different growth times: t_1 = 1 min, t_2 = 5 min, t_3 = 15 min and t_4 = 30 min are presented in parts (a), (b), (c) and (d) of Figure 4, respectively. The insets show the enlarged tilted view of InN nanorods shape. At the early stage of growth, InN nanorods have a pencil-like shape delimited by the semi-polar (1-101) r-planes and non-polar (1-100) m-planes facets, as shown in Figure 4 (a). As the growth proceeds, the (1-101) facet area decreases and the (0001) facet starts to appear with the exposure time to the vapor phase (Figure 4 (b)). At 15 minutes, InN nanorods growth occurs with well-developed (0001) top c-plane facet and (1-100) side m-planes facets. Longer growth time of 30 min results in the appearance of (11-20) side a-planes facets at the bottom part of the nanorods (Figure 4 (d)). The facets which remain after growth had the slowest development. The growth rate of the (1-100) m-planes is low due to HCl and/or H_2 passivation, (1-100) m-planes always limit the final morphology of the rods. Then, there is a competition between the growth rates of the c-plane and r-planes facets.

The axial and radial growth rates of the InN nanorods along (0001) and (1-100) directions, respectively, as a function of the growth time are reported in Figure 4 (e). During the first stages of the growth, the axial and radial growth rates are very fast, about 938 $nm.min^{-1}$ and 114 $nm.min^{-1}$, respectively, for a 1 min growth time. Then they strongly decrease within a short time of 5 min. Finally, they respectively stabilize around 85 $nm.min^{-1}$ and 8 $nm.min^{-1}$.

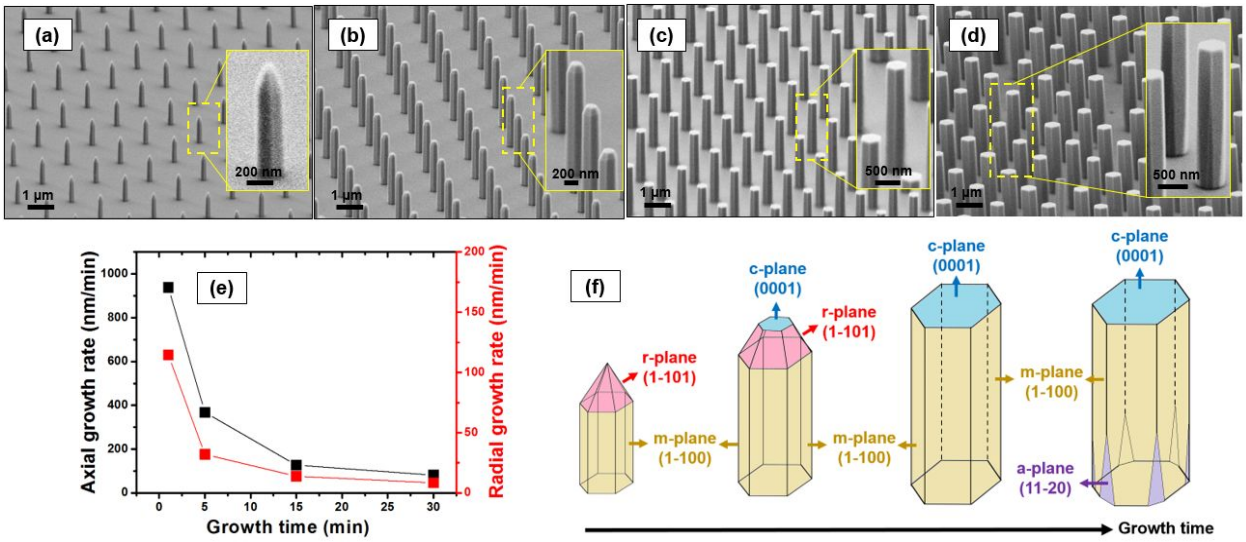

Figure 4: (a) – (d) SEM images of InN nanorods grown on Ga polar GaN/c-Al_2O_3 templates masked by SiN_x at different growth times (a) 1 min , (b) 5 min, (c) 15 min and (d) 30 min. (e) Axial (black) and radial (red) growth rates of InN nanorods as a function of the growth time. (e) Schematic illustration of InN crystal shape evolution as a function of the growth time. The nanorods morphology changes from a pencil-like shape to a hexagonal shape with the growth time.

From these observations and according to Ref [26], we assume that the growth rate is governed by both mass transport and surface kinetics. At the initial stage of the growth, the growing surface area is small and the depletion of the growth precursors in the vapor phase is very limited. The growth rates are then at their maximum and can be considered as kinetically-limited. The growth rate of the (0001) c-plane facet is then greater than those of the (1-101) r-planes and (1-100) m-planes facets, this is the reason why the nanorods have a pencil-like shape at 1 minute. When the growth time increases, the growing surfaces of the nanorods extend gradually due to the positive axial and lateral growth rates. This induces a vapor phase depletion of reacting species near the InN surface that cannot be neglected. The reactive materials that reach the surfaces of the InN rods are then not sufficient. Thus, the growth turns into mass-transport limited. Consequently, the axial growth rate decreases and the top (0001) c-plane facet begins to appear after 5 minutes. Then, the (1-101) r-planes facets, of which growth rate exceeds the growth rate along (0001), disappear (the crystal is now limited by the top c-plane facet) and the hexagonal prism emerges as the dominant structure, as we can see after 15 minutes of growth.

Finally, the appearance of the (11-20) a-planes facets after 30 minutes of growth is the consequence of the decrease of their growth rates with respect to the (1-100) m-planes facets.

- **Optical properties of InN nanorods**

The optical properties of InN nanorods were investigated by photoluminescence (PL) with a continuous laser power of 50 mW. The PL measurements were first performed on nanorod arrays at a temperature of 10 K. Figure 5 exhibits the strong dependence of the PL spectra, in term of intensity, peak energy and linewidth as a function of the growth temperature. For nanorods grown at the lowest temperature (T = 610 °C) only a broad emission centered at 0.85 eV is observed. PL emission of InN nanorods grown at very high temperature (T = 690 °C) has been not detected because of the low quality of the material. The samples grown at T = 640 °C and T = 660 °C, however, exhibit stronger PL emissions centered at 0.77 and 0.76 eV, respectively, with a substantial increase in the PL peak intensity for the sample grown at 660 °C compared to that of sample grown at 640 °C. The nanorods size is higher at 660 °C which may explain the increased PL intensity. These observations are somewhat consistent with previous reported results, where the PL intensity gradually increased with the growth temperature from 440 °C to 525 °C [38]. Moreover, the full width at half maximum (FWHM) of nanorods grown at 640 °C is larger than those obtained at a growth temperature of 660 °C. These observations tend to indicate that InN nanorods grown at 660 °C are of higher quality.

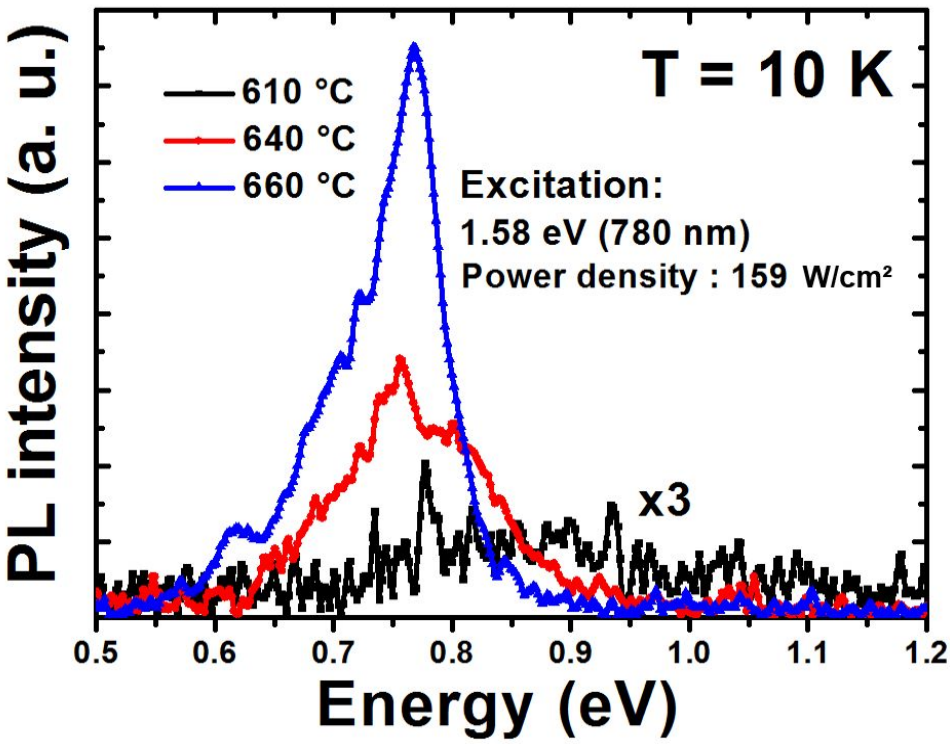

Figure 5 : Photoluminescence spectra at 10 K of InN nanorods grown on patterned GaN/Al_2O_3 templates at different growth temperatures under a laser power density of 159 W/cm².

The PL peak energy (0.76 eV) recorded at low PL temperature (10 K) is significantly larger than the typically measured value of 0.692 eV related to intrinsic InN material. It has been reported that unintentionally-doped InN nanowires emitting at 0.75 eV possess a high electron concentration, around 10^{18} cm^{-3} [39]. For n-type semiconductors, the increase of electron concentration is known to shift the Fermi level into the conduction band leading to an increase of the emission energy through the band-filling Burstein-Moss effect. This high energy of 0.76 eV indicates that our InN nanorods probably contain a significant density of free electrons. The fact that as grown InN material (nanowires, films) are mostly unintentionally n-type with a high residual doping is not really explained. The reported causes of this unintentional doping are nitrogen vacancies, monatomic hydrogen and other impurities [40], [41], [42]. As previously shown, nitride materials grown by HVPE contain small amount of Si, coming from the hot quartz wall of the reactor, yielding a residual n-type doping [43]. On the other hand, several studies evidence the presence of an electron accumulation layer on polar and non-polar planes of both InN films and

nanorods [25], [39], [44], [45]. It is assumed that this accumulation layer is due to surface states (density of positive charge), which are intrinsic of InN surfaces, and to doping mechanisms which are thickness-dependent [46], [47]. Segura-Ruiz *et al*. have shown that the effect of the surface electron accumulation layer on the optical band gap of InN nanocolumn grown by MBE is more pronounced when the diameter decreases [25]. Ahn *et al.* have revisited these findings through a detailed study comparing the optical properties of InN film and nanorods with different diameters [24]. This may explain, in part, the high peak energy of 0.85 eV recorded from the InN nanorods grown at 610 °C, which present small diameters.

In order to understand the nature of the InN nanorod PL, temperature-dependent PL experiments have been carried out from 10 to 300 K on the sample grown at 660 °C. It is shown that the emission spectra depend critically on the PL temperature. The temperature-dependent peak energy of InN nanorods plotted in Figure 6 (b) strongly differs from the Varshni-like temperature dependence of the InN bandgap energy. Due to the high free electron density on the lateral surfaces, the carrier redistribution on the electronic states is greatly inhomogeneous and reveals an anomalous behavior of the peak energy and FWHM as a function of temperature. When the PL temperature increases, the generated photoholes in the inner core can move over a deeper region and recombine with electrons in the surface accumulation layer which provides a blueshift followed by a noticeable broadening of the PL peak. The normal redshift induced by the temperature dependence of the band gap, which is always present, can compensate the blueshift, consequently the PL peak energy appears to be independent of the temperature. The variation in the density of the positive charge at the nonpolar surfaces from a nanorod to another can also induce a noticeable broadening of the PL spectra [25].

The thermal quenching of PL peak intensity can be fitted by the following equation:

$$I(T) = \frac{I_0}{1 + A\exp\left(-\frac{E_a}{k_B T}\right) + B\exp\left(-\frac{E_b}{k_B T}\right)} \quad (3)$$

where E_a and E_b denote the thermal activation energies at low and high temperatures, respectively, A and B are the fitting constants, I_0 is the PL peak intensity at 10 K and and k_B is the Boltzmann's constant. The Arrhenius plot of $I(T)/I_0$ as a function of 1/T is displayed in Figure

6 (c). Fitting the equation (3) gives E_a and E_b respectively equal to 11 ± 1.5 meV and 31 ± 1.5 meV. The activation energy of 11 meV at low temperature can be attributed to structural defects in our nanorods. The binding energy of the localized hole states considered as acceptor like centers in the n-type region can be extracted from the half-amplitude energy ($E_{1/2}$) from the PL spectra at low temperature [48]. We estimate the binding energy of these acceptor like centers to be 40 meV, in rather good agreement with the value of 31 ± 1.5 meV determined through PL experiments as a function of temperature. Our experimental observation is also very close to previously reported experimental values in the range of ~ 25-50 meV, which are associated to impurities [24], [25]. The n concentration deduced from the analysis of the low temperature spectrum related to the sample grown at 660 °C is about 2.6 x 10^{18} cm^{-3}.

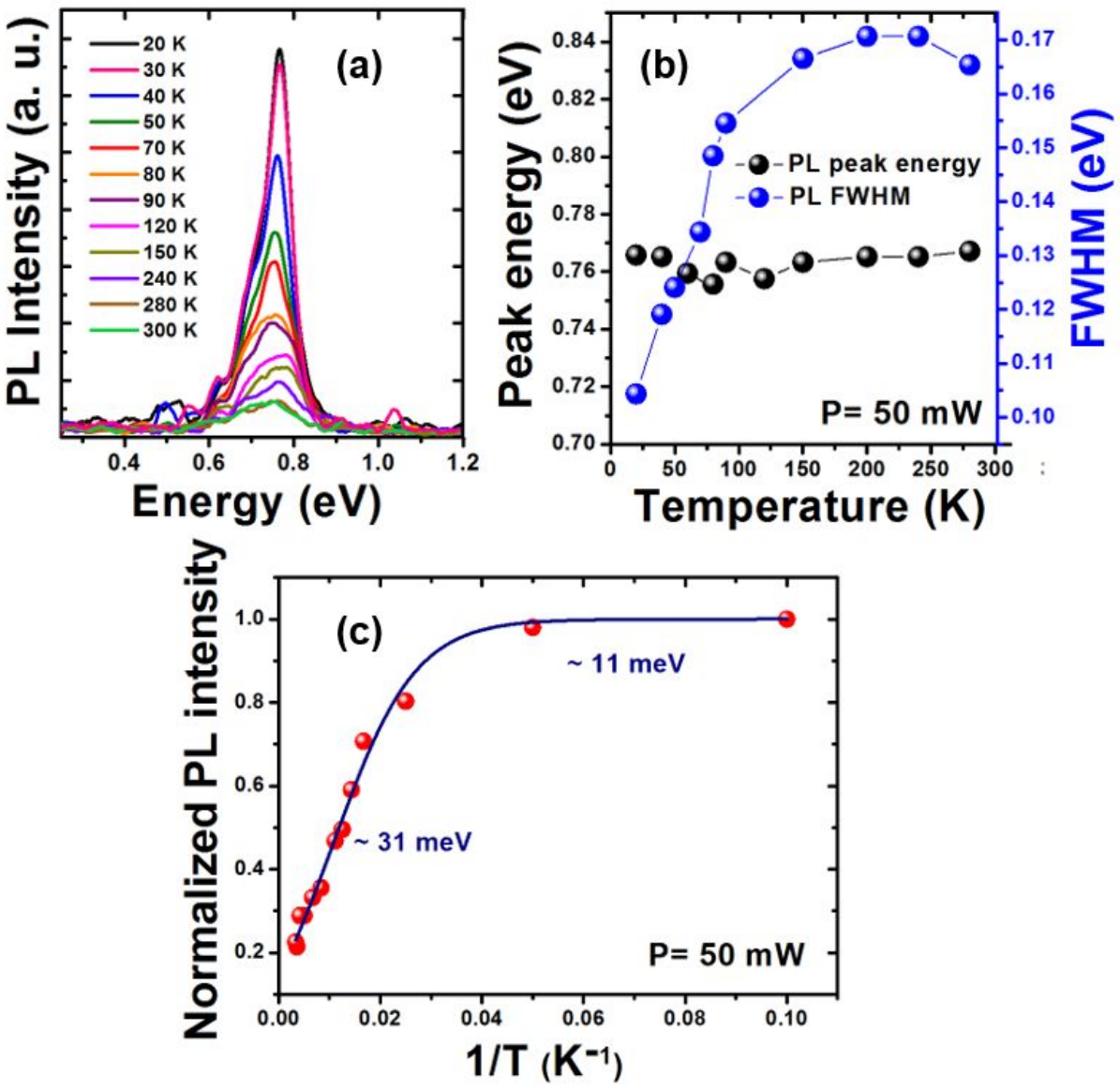

Figure 6: Temperature dependence of (a) PL intensity and (b) PL peak energy and PL bandwidths of InN nanorods grown on patterned GaN/Al_2O_3 templates at 660 °C. (c) Normalized intensity variation of the PL intensity as a function of the reciprocal temperature.

4. Conclusion

In this work the selective area growth (SAG) of InN nanorods on sapphire substrates with a Ga-polar GaN buffer layer was explored. We showed that the selectivity and the nanorods morphology depend strongly on the growth temperature. The effect of the input NH_3 on the

growth rates and the shape of nanorods was investigated. It revealed that the hydrogen species, generated from NH_3 decomposition, have a significant impact on the supersaturation of InN deposition. The effect of the mass transport in the vapor phase on the growth rate is found to be more significant at larger growth time. The nanorod morphology can be simply tuned from pencil to a perfect hexagonal shape by changing the growth conditions. The optical quality of HVPE-grown InN rods is assessed by PL measurements which reveal a good agreement with high quality MBE-grown InN nanowires. These results highlight the potential of the HVPE process to achieve SAG of well-controlled arrays of InN nanorods. HVPE appears to be a relevant promising growth technique for future InN nanorods based-devices.

Author contributions

The manuscript was written through contributions of all authors. All authors have given approval to the final version of the manuscript.

Acknowledgement

The financial support received from CNRS (PRC1300 CNRS-JSPS) and from GaNeX program of the French ANR agency (ANR-11-LABX-0014) are gratefully acknowledged. This work was also funded by the program "Investissements d'avenir" of the French ANR agency, the French governement IDEX-SITE initiative 16-μIDEX-0001 (CAP20-25), the European Commission (Auvergne FEDER Funds) and the Region Auvergne in the framework of the LabEx IMobS3 (ANR-10-LABX-16-01) and CPER. The authors thank 2MAtech, Aubiere, France for scanning electron microscopy measurements.

Corresponding authors

*Mohammed ZEGHOUANE. Institut Pascal, 4 Avenue Blaise Pascal, 63178 Aubière Cedex. France.

E-mail: mohammed.zeghouane@uca.fr

*Agnès TRASSOUDAINE. Institut Pascal, 4 Avenue Blaise Pascal, 63178 Aubière Cedex. France.

E-mail: agnes.trassoudaine@uca.fr

References

[1] Ambacher, O. Growth and applications of Group III-nitrides. *J. Phys. D: Appl. Phys*. **1998**, 31, 2653.

[2] Bhuiyan, A. G.; Hashimoto, A.; Yamamoto, A. Indium nitride (InN): A review on growth, characterization, and properties. *Journal of Applied Physics*. **2003**, 94, 2779-2808.

[3] Mohammad, S. N.; Morkoc, H. Progress and prospects of group-III nitride semiconductors. *Prog. Quantum Electron.* **1996**, 20, 361–525.

[4] Mi, Z.; Zhao, S. Extending group-III nitrides to the infrared: Recent advances in InN. *Phys. Status Solidi B.* **2015**, 252, 1050.

[5] Lye, K. S.; Kobayashi, A.; Ueno, K.; Ohta, J.; Fujioka, H. InN thin-film transistors fabricated on polymer sheets using pulsed sputtering deposition at room temperature. *Appl. Phys Lett.* **2016**, 109, 032106.

[6] Hsu, L. H.; Kuo, C. T.; Huang, J. K.; Hsu, S. C.; Lee, H. Y.; Tsai. Y. L.; Su, C. F.; Lin, C. C. InN-based heterojunction photodetector with extended infrared response. *Opt. Express*, **2015**, 23, 31150-31162.

[7] Syrkin, A.; Usikov, A.; Soukhoveev, V.; Kovalenkov, O.; Ivantsov, V.; Dmitriev, V.; Holtz, M. InN-based layers grown by modified HVPE, *phys. stat. sol.* **2006**, 6, 1444–1447.

[8] Suihkonen, S.; Sormunen, J.; Rangel-Kuoppa, V.T.; Koskenvaara, H.; Sopanen, M. J. Growth of InN by vertical flow MOVPE. *Cryst. Growth*. **2006**, 291, 8–11.

[9] Kumar, M.; Rajpalke, M. K.; Bhat, T. N.; Roul, B.; Sinha, N.; Kalghatgi, A. T.; Krupanidhi, S. B. Growth of InN layers on Si (111) using ultra-thin silicon nitride buffer layer by NPA-MBE. *Mater. Lett*. **2011**, 65, 1396–1399.

[10] Jain, A.; Weng, X.; Raghavan, S.; Vanmil, B. L.; Myers, T.; Redwing, J. M.; Vanmil, B. L. Redwing, J. M. Effect of polarity on the growth of InN films by metalorganic chemical vapor deposition. *J. Appl. Phys*. **2008**, 104, 053112.

[11] Wang, K.; Araki, T.; Takeuchi, M.; Yoon, E.; Nanishi, Y.; Wang, K.; Nanishi, Y. Selective growth of N-polar InN through an in situ AlN mask on a sapphire substrate. *Appl. Phys. Lett*. **2014**, 104, 032108.

[12] Zhao, S.; Mi, Z. Chapter Eight - InN Nanowires: Epitaxial Growth, Characterization, and Device Applications. *Semicond. Semimetals*. **2017**, 96, 267-304.

[13] Calleja, E.; Ristić, J.; Fernández-Garrido, S.; Cerutti, L.; Sánchez-García, M. A.; Grandal, J.; Trampert, A.; Jahn, U.; Griol, A.; Sánchez, B. Growth, morphology, and structural properties of group-III-nitride nanocolumns and nanodisks. *Phys. stat. sol. (b)*, **2007**, 244, 2816-2837.

[14] Ahn, H.; Ku, Y.; Wang, Y.; Chuang, C.; Gwo, S.; Pan, C.; Chuang, C. Terahertz emission from vertically aligned InN nanorod arrays. *Appl. Phys. Lett*. **2007**, 91, 132108.

[15] Durand, C.; Bougerol, C.; Carlin, J. F.; Rossbach, G.; F. Godel, Eymery, J.; Jouneau, P. H., Mukhtarova, A.; Butté, R.; Grandjean, N. M-Plane GaN/InAlN Multiple Quantum Wells in Core–Shell Wire Structure for UV Emission. *ACS photonics*. **2014**, 1(1), 38-46.

[16] Brandt, O.; Pfüller, C.; Chèze, C.; Geelhaar, L.; Riechert, H. Sub-meV linewidth of excitonic luminescence in single GaN nanowires: Direct evidence for surface excitons. *Physical review b*. **2010**, 81, 045302.

[17] Flissikowski, T.; Brandt, O.; Grahn, H. T.; Geelhaar, L.; Riechert, H. Suitability of Au- and Self-Assisted GaAs Nanowires for Optoelectronic Applications. *Nano Lett*. **2011**, 11(3), 1276–1279.

[18] Harui, S.; Tamiya, H.; Akagi, T.; Miyake, H.; Nanishi, Y. Transmission electron microscopy characterization of position-controlled InN nanocolumns. *Jpn. J. Appl. Phys* **2008**, 47, 5330–5332.

[19] Kamimura, J.; Kishino, K.; Kikuchi. A. Dislocation reduction via selective-area growth of InN accompanied by lateral growth by rf-plasma-assisted molecular-beam epitaxy. *Appl. Phys. Lett*. **2010**, 97, 141913.

[20] Liang, C. H.; Chen, L. C.; Hwang, J. S.; Chen, K. H.; Hung, Y. T.; Chen, Y. F. Selective-area growth of indium nitride nanowires on gold-patterned Si(100) substrates. *Appl. Phys. Lett* **2002**, 81, 22.

[21] Wang, X.; Zhang, G.; Xu, Y.; Wu, H.; Liu, C. Selective-Area Growth of Transferable InN Nanocolumns by Using Anodic Aluminum Oxide Nanotemplates. *Nanoscale Res. Lett.* **2017**, 12, 145.

[22] Zeghouane, M.; Avit, G.; Cornelius, T. W, André, Y.; Bougerol, C.; Taliercio, T.; Ferret, P.; Gil, E.; Tournié, E.; Thomas. O.; Trassoudaine. A.; Selective Growth of Ordered Hexagonal InN Nanorods *CrystEngComm***, 2019**, 21, 2702-2708.

[23] Chang, C. Y.; Chi, G. C.; Wang, W. M.; Chen, L. C.; Chen, K. H.; Ren, F.; Pearton, S. J. Electrical transport properties of single GaN and InN nanowires. *Journal of Electronic Materials*, **2006**, 35, 738-743.

[24] Ahn, H.; Liu, Y. S.; Chang, K. Y.; Gwo, S. Photoluminescence from InN Nanorod Arrays with a Critical Size. *Appl. Phys. Express*, **2013**, 6, 062103.

[25] J. Segura-Ruiz, J.; Garro, N.; Cantarero, A.; Denker, C.; Malindretos, J.; Rizzi, A. Optical studies of MBE-grown InN nanocolumns: Evidence of surface electron accumulation. *Phys. Rev. B*, **2009**, 79, 115305.

[26] Avit, G.; Zeghouane, M.; André, Y.; Castelluci, D.; Gil, E.; Baé, S. Y.; Amano, H.; Trassoudaine, A. Crystal engineering by tuning the growth kinetics of GaN 3-D microstructures in SAG-HVPE. *Cryst Eng Comm* **2018**, 20, 6207-6213.

[27] Lekhal, K.; Bae, S. Y.; Lee, H. J.; Mitsunari, T.; Tamura, A.; Deki, M.; Honda, Y.; Amano, H. Selective-area growth of GaN microrods on strain-induced templates by hydride vapor phase epitaxy. *Jpn. J. Appl. Phys* **2016**, 55-05FF03.

[28] Li, H.; Geelhaar, L.; Riechert, H.; Draxl, C.; Computing Equilibrium Shapes of Wurtzite Crystals: The Example of GaN. Phys. *Rev. Lett*. **2015**, 115, 085503.

[29] Gacevic, Z.; Sanchez, D. G.; Calleja. E. Formation Mechanisms of GaN Nanowires Grown by Selective Area Growth Homoepitaxy. *Nano Lett*. **2015**, 15, 1117−1121.

[30] Wang, X.; Hartmann, J.; Mandl, M.; Mohajerani, M. S.; Wehmann, H. H.; Strassburg, M.; Waag, A.; Growth kinetics and mass transport mechanisms of GaN columns by selective area metal organic vapor phase epitaxy. *J. Appl. Phys*. **2014**, 115, 163104.

[31] Lundskog, A.; Forsberg, U.; Holtz, P. O.; Janzen, E. Morphology Control of Hot-Wall MOCVD Selective Area Grown Hexagonal GaN Pyramids. *Cryst. Growth Des*. **2012**, 12, 5491−5496.

[32] Hersee, S. D.; Sun, X.; Wang, X. The Controlled Growth of GaN Nanowires. *Nano Lett*. **2006**, 6, 8, 1808-1811.

[33] Bengoechea-Encabo, A.; Barbagini, F.; Fernández-Garrido, S.; Grandal, J.; Ristic, J.; Calleja, E.; Jahn, U.; Luna, E.; Trampert, A.; Understanding the selective area growth of GaN nanocolumns by MBE using Ti nanomasks. *J. Cryst. Growth*, **2011**, 325, 89–92.

[34] Zeghouane, M.; Avit, G.; André, Y.; Bougerol, C.; Ferret, P.; Gil, E.; Amano, H.; Trassoudaine. A. Compositional control of homogeneous InGaN nanowires with the In content up to 90%, **2019**, *Nanotechnology*, 30, 044001.

[35] Kumagai, Y.; Takemoto, K.; Koukitu, A.; Hisashi, S. Thermodynamics on halide vapor-phase epitaxy of InN using InCl and $InCl_3$. *J. Cryst. Growth*. **2001**, 222, 118-124.

[36] Lymperakis, L.; Neugebauer J.; Himmerlich M.; Krischok, S.; Rink, M.; Kröger, J.; M. Polyakov, V. Adsorption and desorption of hydrogen at nonpolar GaN (1-100) surfaces: Kinetics and impact on surface vibrational and electronic properties. *Physical Review B,* **2017***,* 95, 195314.

[37] Li, S. F.; Fuendling, S.; Wang, X.; Merzsch, S.; Wei J. D.; Waag, A. Polarity and Its Influence on Growth Mechanism during MOVPE Growth of GaN Sub-micrometer Rods. Cryst. Growth Des. **2011**, 11, 1573–1577.

[38] Stoica T.; Meijers, R.; Calarco, R.; Richter, T.; Luth, H. MBE growth optimization of InN nanowires. *J. Cryst. Growth*. **2006**, 290, 241-247.

[39] Stoica T.; Meijers, R.; Calarco, R.; Richter, T.; Sutter, E.; Luth, H. Photoluminescence and Intrinsic Properties of MBE-Grown InN Nanowires. *Nano Lett*, **2006**, 7, 1541-1547.

[40] Piper, L. F. J.; Veal, T. D.; McConville, C. F.; Lu, H.; Schaff, X. J.; Origin of the n-type conductivity of InN: The role of positively charged dislocations, *Appl. Phys. Lett*, **2006**, 88, 252109.

[41] Janotti, A.; Van de Walle, C. G. Sources of unintentional conductivity in InN. Appl. Phys. Lett. **2008**, 92, 032104

[42] Mahboob, I.; Veal, T. D.; McConville, C. F.; Lu, H.; Schaff, W. J. Intrinsic Electron Accumulation at Clean InN Surfaces. *Phys. Rev. Lett*. **2004**, 92, 036804

[43] Fujito, K.; Kubo, S.; Nagaoka, H; Mochizuki, T.; Namita, H. Bulk GaN crystals grown by HVPE. *J. Cryst. Growth.* **2009**, 311, 3011-3014.

[44] Mahboob, I.; Veal, T. D.; McConville, C. F.; Lu, H.; Schaff, W. J. Intrinsic Electron Accumulation at Clean InN Surfaces. *Phys. Rev. Lett*. **2004**, 92, 036804.

[45] Calleja, E.; J. Grandal, J.; M. A. Sánchez-García, M. A. Evidence of electron accumulation at nonpolar surfaces of InN nanocolumns. *Appl. Phys. Lett*. **2007**, 90, 262110.

[46] Cimalla, V.; Lebedev, V.; Morales, F. M.; Goldhahn, R.; Ambacher, O. Model for the thickness dependence of electron concentration in InN films. *Appl. Phys. Lett*, **2006**, 89, 172109

[47] V. Darakchieva, V.; Hofmann, T.; Schubert, M.; Sernelius, B. E.; Monemar, B.; Giuliani, F.; Alves, E.; Lu, H.; Schaff, W. J. Free electron behavior in InN: On the role of dislocations and surface electron accumulation. *Appl. Phys. Lett.* **2009**, *94*, 022109.

[48] DeSheng, J.; Makita, Y.; Ploog, K.; Queisser, H. J. Electrical properties and photoluminescence of Tedoped GaAs grown by molecular beam epitaxy. *J. Appl. Phys*. 1982, 53, 999.

"For Table of Contents Use Only"

Morphological control of InN nanorods by SAG-HVPE

Mohammed Zeghouane, *Geoffrey* Avit, *Yamina* André, *Thierry* Taliercio, *Pierre* Ferret, *Evelyne* Gil, *Dominique* Castelluci, *Pierre* Disseix, *Joel* Leymarie, *Eric* Tournié, and *Agnès* Trassoudaine

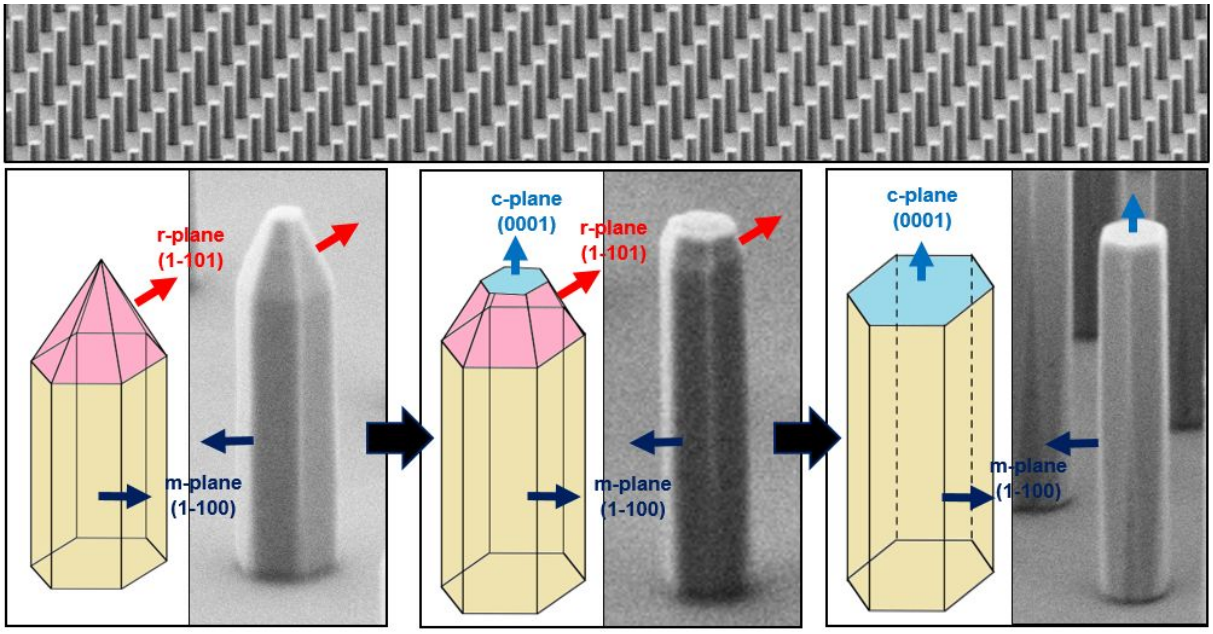

The selective epitaxy of hexagonal InN nanorods by HVPE is now well understood: the hierarchy of growth rates of the different facets according to the experimental parameters is determined and the physical phenomena involved are identified.

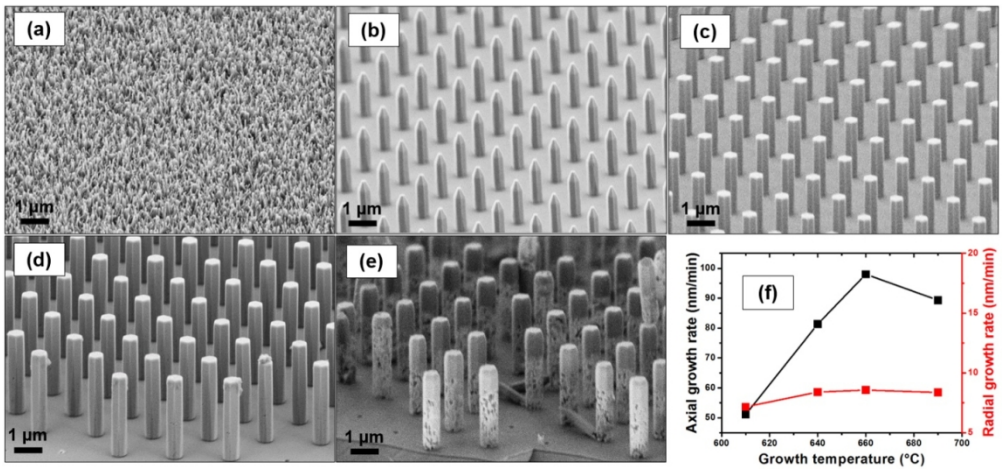

Figure 1: (a) – (e) SEM images of InN nanorods grown on Ga polar GaN/c-Al2O3 templates masked by SiNx at growth temperatures of (a) 580 °C, (b) 610 °C, (c) 640 °C, (d) 660 °C and (e) 690 °C. (f) Axial (black) and radial (red) growth rates of InN nanorods as a function of the growth temperature. The selectivity is achieved from 610 °C. The higher growth temperature of 690 °C results in InN crystal deterioration.

264x135mm (138 x 125 DPI)

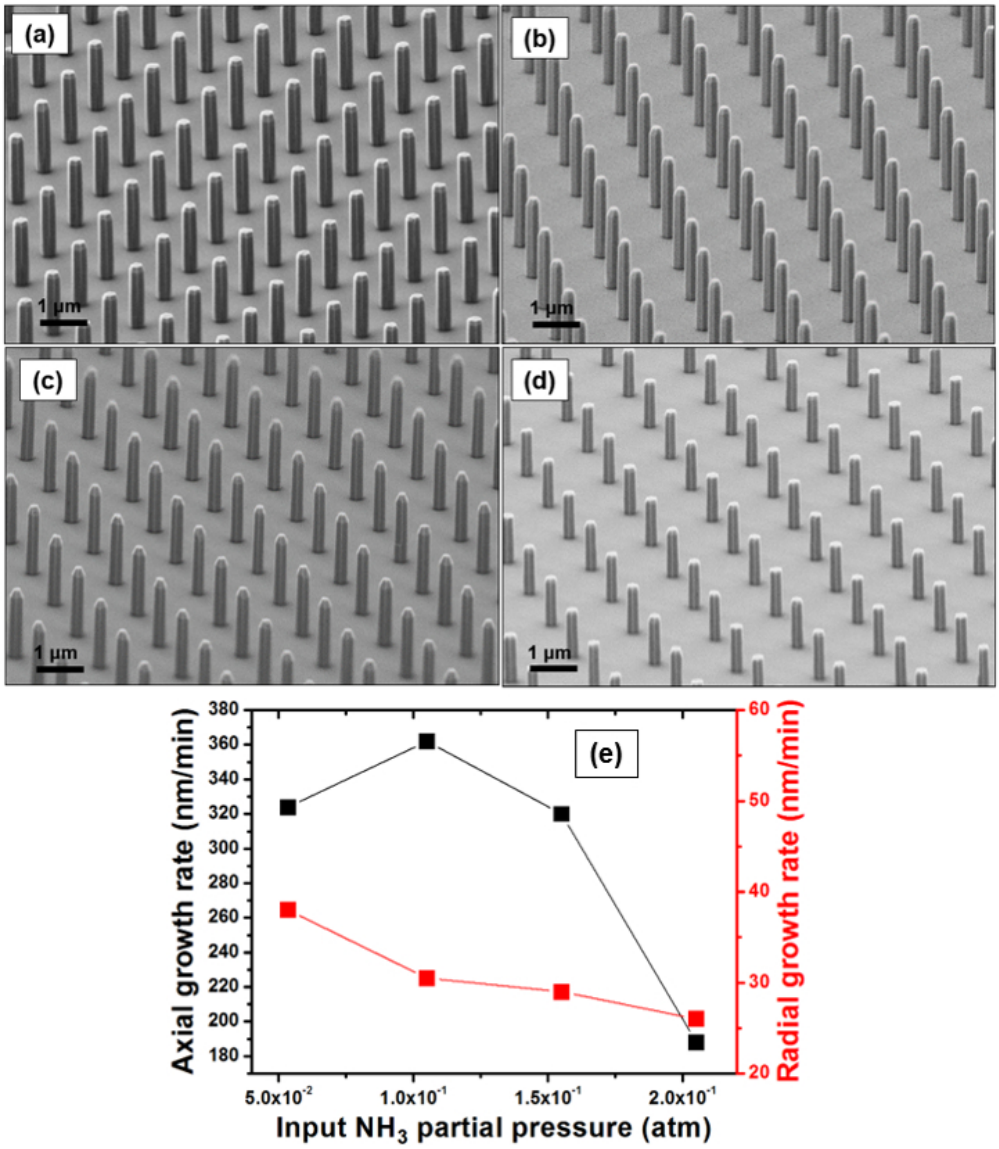

Figue 2: (a) – (d) SEM images of InN nanorods grown on Ga polar GaN/c-Al2O3 templates masked by SiNx at different input NH3 partial pressures (a) 5.00 x 10-2 atm, (b) 1.00 x 10-1 atm, (c) 1.50 x 10-1 atm and (d) 2.00 x 10-1 atm. (e) Axial (black) and radial (red) growth rates of InN nanorods as a function of the input NH3 partial pressure. Nanorods growth rate and morphology depend on the introduced partial pressure of NH3.

183x212mm (100 x 99 DPI)

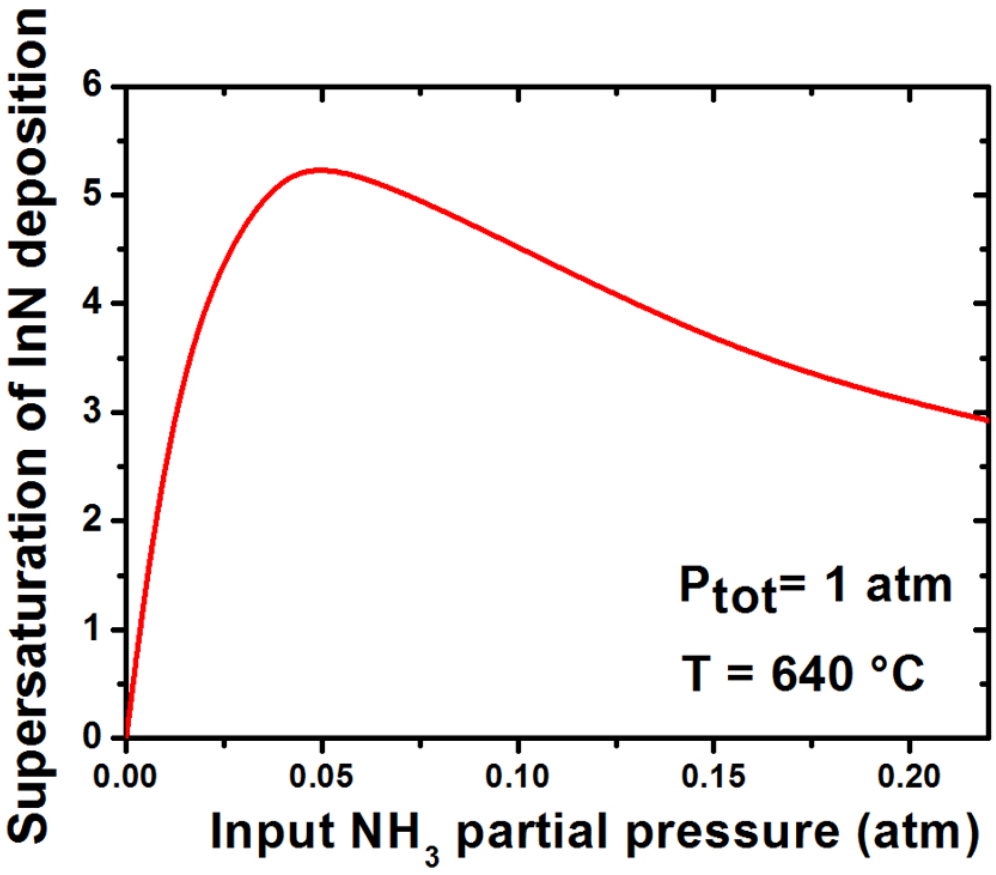

Figure 3: Plot of the supersaturation parameter for InN deposition as a function of the input NH3 partial pressure. Ptot is the total pressure in the reactor. The supersaturation in the vapor phase to promote InN deposition decreases at higher P0NH3.

141x123mm (150 x 150 DPI)

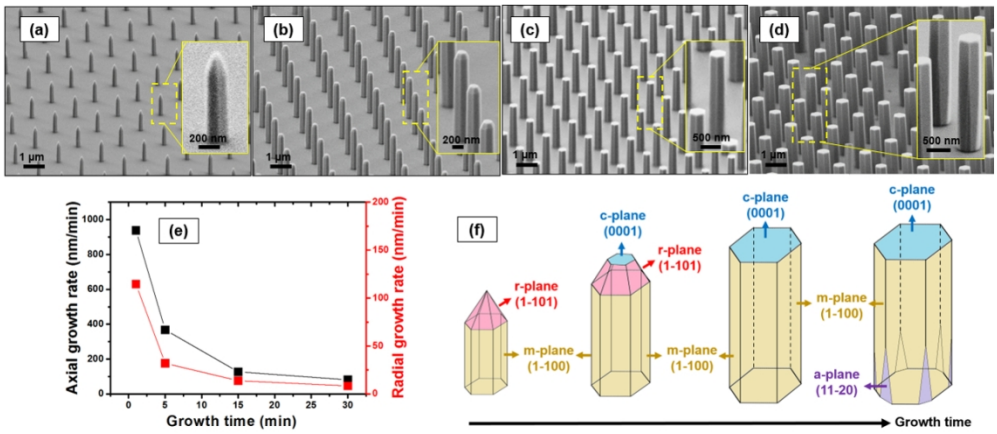

Figure 4: (a) – (d) SEM images of InN nanorods grown on Ga polar GaN/c-Al2O3 templates masked by SiNx at different growth times (a) 1 min , (b) 5 min, (c) 15 min and (d) 30 min. (e) Axial (black) and radial (red) growth rates of InN nanorods as a function of the growth time. (e) Schematic illustration of InN crystal shape evolution as a function of the growth time. The nanorods morphology changes from a pencil-like shape to a hexagonal shape with the growth time.

271x134mm (121 x 105 DPI)

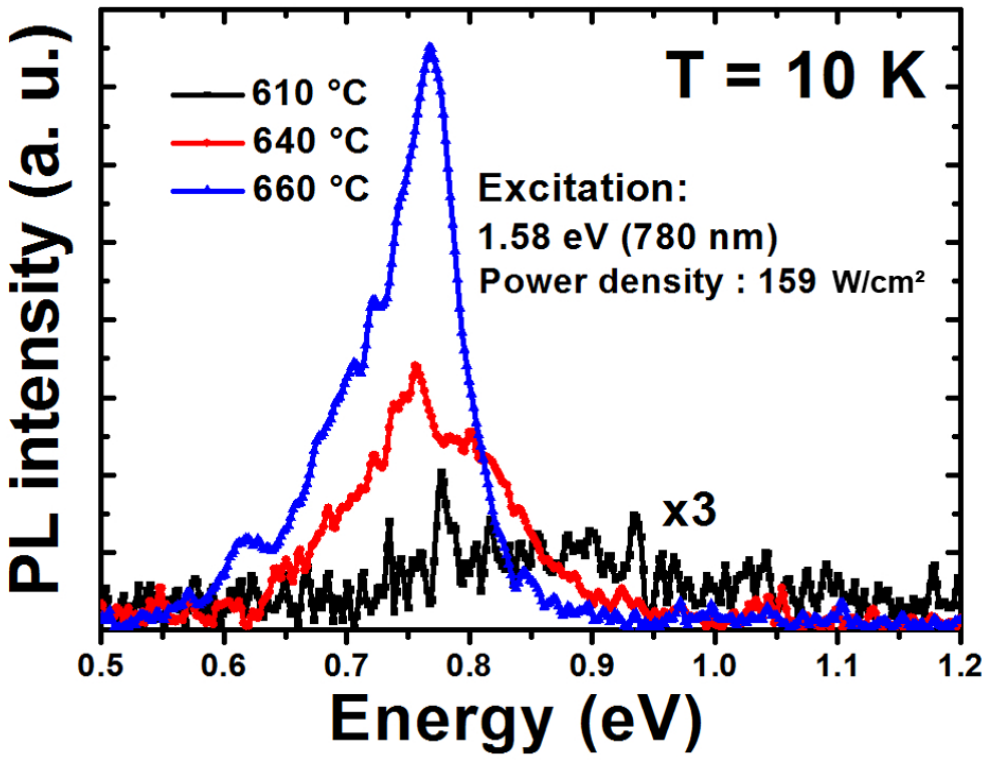

Figure 5 : Photoluminescence spectra at 10 K of InN nanorods grown on patterned GaN/Al2O3 templates at different growth temperatures under a laser power density of 159 W/cm².

193x150mm (124 x 123 DPI)

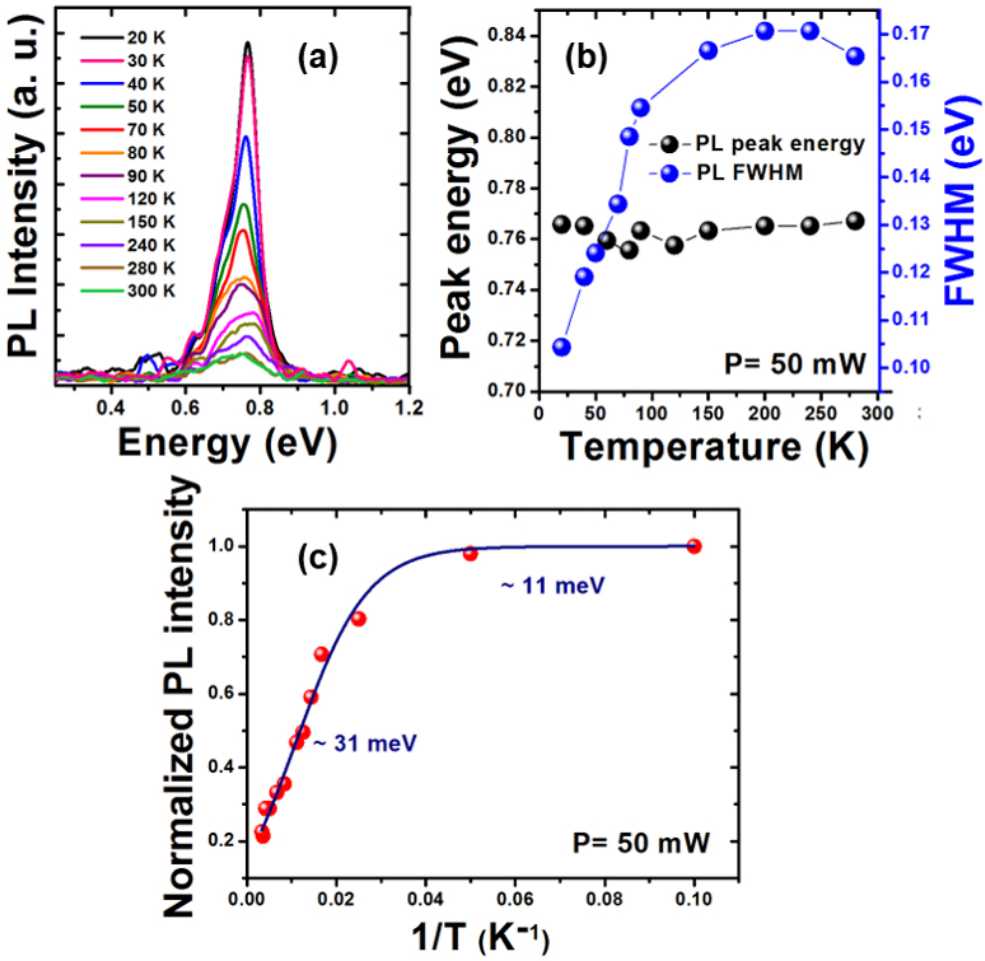

Figure 6: Temperature dependence of (a) PL intensity and (b) PL peak energy and PL bandwidths of InN nanorods grown on patterned GaN/Al2O3 templates at 660 °C. (c) Normalized intensity variation of the PL intensity as a function of the reciprocal temperature.

181x173mm (110 x 113 DPI)